Rigidity of Triskelion Arms and Clathrin Nets

Albert J. Jin* and Ralph Nossal†

*Laboratory of Physical Biology, National Institute of Arthritis and Musculoskeletal and Skin Diseases, and †Laboratory of Integrative and Medical Biophysics, National Institute of Child Health and Human Development, National Institutes of Health, Bethesda, Maryland 20892 USA

ABSTRACT Statistical analysis is applied to a set of electron micrographic images (Kocsis, E., B. L. Trus, C. J. Steer, M. E. Bisher, and A. C. Steven. 1991. *J. Struct. Biol.* 107:6–14), from which quantitative measures are obtained to support the notion that the three arms of a triskelion have statistically identical properties and exhibit independent structural fluctuations. Additionally, a study of local contour fluctuations, which indicates that the elastic properties of a triskelion arm are approximately constant over the entire arm length, is used along with a small deformation statistical mechanics theory to derive an effective, average flexural rigidity for the arms. This result is used to estimate the bending energy necessary to deform a clathrin patch, and comparison is made with the deformation energy of an equivalent area of non-clathrin-coated membrane. We estimate that the rigidity of the clathrin lattice is at least comparable to that of a typical membrane. Hence, the natural curvature of a clathrin cage can stabilize, and perhaps propel, the formation of intracellular coated vesicles.

INTRODUCTION

Various proteins are known to be implicated in the budding of vesicles from the membranes of eucaryotic cells (Schmid, 1993, 1997; Parton, 1996; Schekman and Orci, 1996; Robinson et al., 1996; Anderson, 1998; Dell'Angelica et al., 1998). The best characterized is clathrin, which appears in a cell as a three-armed heteropolymer referred to as a clathrin *triskelion.* In moderately acidic solutions, triskelions spontaneously assemble to form closed polyhedra (cages) that are morphologically similar to the coats of certain vesicles that can be harvested from a variety of tissues and cells (Woodward and Roth, 1978; Keen et al., 1979; Crowther and Pearse, 1981; Kirchhausen and Harrison, 1981). Native clathrin coats and clathrin-coated vesicles have been studied most in the context of receptor-mediated endocytosis, which is the process by which many materials are taken up into cells by binding to specific receptors that lie across the plasma membrane. These embedded receptors, with their bound ligand, associate with "adaptins" (also, variously known as APs or "assembly proteins"), possibly via activated AP membrane binding sites (Santini et al., 1998). The APs, in turn, bind to clathrin on the cytoplasmic face of the membrane (Vigers et al., 1986; Keen, 1990; Robinson, 1992). Other proteins, such as the GTPase dynamin (Sweitzer and Hinshaw, 1998) and the dynamin-associated protein amphiphysin (Takei et al., 1999), are involved transiently in various steps of clathrin-coated vesicle formation, but their structural roles in the liberated vesicle are not well established.

The primary function of the clathrin coat is yet to be definitively resolved. One hypothesis is that clathrin, through its interaction with accessory-protein-linked receptors, acts to concentrate cargo in the interior of a budding vesicle. Another possibility is that coat proteins might destabilize membranes by acting as molecular surfactants to release elastic energy stored in a lipid bilayer (Oster et al., 1989). Yet another proposal is that the polymerized clathrin basket, through its natural curvature, imparts tension in the plasma membrane and thereby drives the membrane from a structure of low average curvature to one having the high curvature of a small vesicle. However, for a clathrin lattice to drive vesiculation, its stiffness must be comparable to, or larger than, that of the cell membrane. To see whether an assembled clathrin lattice can, in this way, influence vesicle formation, we here shall estimate the rigidity of a clathrin patch and compare it to that of a typical biological membrane.

Direct mechanical measurements provide values for the rigidities of biological membranes (Evans, 1983; Elson, 1988; Frank, 1990; Zhelev et al., 1994). To estimate the rigidity of a clathrin coat, we examine conformation fluctuations of isolated triskelions by using techniques similar to those that have been used to determine the bending moduli of microtubules and actin filaments (Gittes et al., 1993; Käs et al., 1996). The latter structures are large enough to be observed optically, but clathrin triskelions are too small and other techniques must be used. To this end, we have obtained a digitized collection of electron microscope images of isolated triskelions (Kocsis et al., 1991), from which we infer that a triskelion behaves as a simple elastic element fluctuating in a viscous medium. Analyses of these images provide characterizations of the average (mean) conformation of triskelion arms and local fluctuations about that mean shape. From the mode magnitudes of the fluctuations along the arms we estimate the arm rigidity and use that information to calculate the bending energy of a clathrin network.

Received for publication 1 December 1998 and in final form 3 December 1999.

Address reprint requests to Dr. Ralph J. Nossal, NIH, Bldg. 12A, Rm. 2041, Bethesda, MD 20892. Tel.: 301-435-9233; Fax: 301-496-2172; E-mail: rjn@helix.nih.gov.

0006-3495/00/03/1183/12 $2.00

In the following, we briefly describe the procedure used to derive a set of digitized electron microscopy images of individual triskelions. We then introduce the notion of a nanoscopic, multivariate probability density for the coordinates of projected shape descriptors of the arms and present inferences based on statistical analyses of triskelion-shape fluctuations. We follow by introducing a method, based on concepts of equilibrium statistical mechanics, that allows us to estimate a value for the planar bending modulus of a triskelion arm. The stiffness of a clathrin lattice patch then is inferred and found to be comparable to that of an equivalent area of typical phospholipid membrane. Various details of analytical methodology are given in appendices.

TRISKELIAL STRUCTURE AND SHAPE DESCRIPTIONS

The standard model for triskelions consists of: 1) a central hub of radius 40 Å; 2) three arms, each of ~520 Å in length and of ~20 Å radius; and 3) three globular domains of radius 36 Å that terminate the three arms. This structural model of triskelions helps explain qualitative geometric and topological features of the packing of triskelions into coated pits and vesicles (Pearse and Bretscher, 1981; Kirchhausen et al., 1987; Pearse and Crowther, 1987; Heuser, 1989; Jin and Nossal, 1993; Smith et al., 1998). Each arm of a native triskelion contains one clathrin heavy chain (~190 kDa) and one tightly, but noncovalently, associated light chain (~23–27 kDa) (Ungewickell and Branton, 1981; Pastan and Willingham, 1985; Brodsky, 1988). Heavy chains belong to a single class and seem to be well conserved across species (Kirchhausen et al., 1987); their carboxyl ends are noncovalently anchored to each other at the central hub. Light chains exist as two classes containing variable functional domains, and are much less conserved (Brodsky et al., 1991). It is believed that heavy chains are primarily responsible for triskelion conformational properties and clathrin network formation, whereas the light chains may enter into molecular interactions between clathrin and other macromolecules involved in endocytosis, with a specificity deriving from the variable light chain domains (Kirchhausen et al., 1987; Brodsky et al., 1991; Lin et al., 1991; Schmid and Smythe, 1991).

The primary data (Kocsis et al., 1991) used in this study are 72 digitized images of intact triskelions (examples are shown in Fig. 1). The clathrin specimens were prepared on mica substrates by the glycerol nebulization/rotary shadowing procedure (Elliott et al., 1976; Shotten et al., 1979). From digitized nodal positions (~8–14 nodes along each arm) we reconstructed, for our analysis, those images of intact triskelia that display clear clockwise vorticity and represent the majority of all images [see Trus and Steven (1981) and Kocsis et al. (1991) for a discussion of initial image processing].

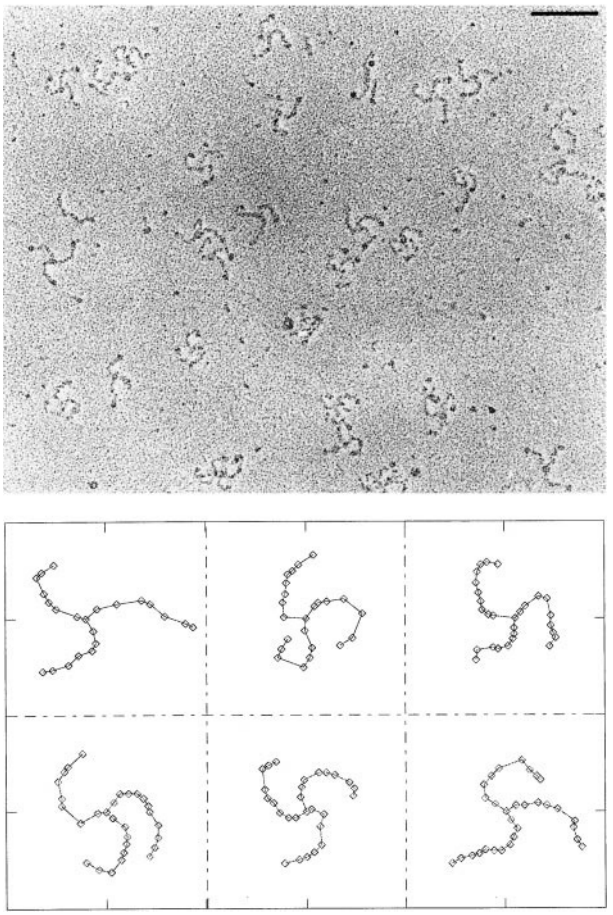

FIGURE 1 Variable shapes of triskelions. (*Top*) electron micrograph of triskelions on mica substrate, obtained by Kocsis and co-workers (1991) via a glycerol nebulization/rotary shadowing procedure. Horizontal bar measures 50 nm in length. (*Bottom*) selected triskelion images, constructed from corresponding digitized node coordinates supplied by Kocsis et al. (1991), where the size of square grids is 50 nm × 50 nm. In the present work we analyze a set of 72 such shape profiles.

Shape variations of the triskelions are described via arm contour lengths and tangential angles, determined from a set of natural cubic spline functions (see Appendix A). Several quantities characterize the fluctuations. Among these (see Fig. 2) are the linear ("straight-line," scalar) distances between the hub and centers of the three terminal domains $\{D_{\mathrm{he}}^{(\mathrm{i,j})}\}$ (where $i = 1, 2, 3$ is the arm index and $j = 1, 2, \ldots, N$ identifies a particular triskelion) and the linear distances between apposing terminal domains $\{D_{\mathrm{ee}}^{(\mathrm{i,j})}\}$ (i.e., between arms i' and i'', $i' \neq i'' \neq i$). We thus are able to compute the frequency distributions of global parameters such as the apparent arm lengths $\{L^{(\mathrm{i})}\}$, the hub angles $\{\phi^{(\mathrm{i})}\}$, the cumulative angles from the hub to terminal domains $\{\theta_{\mathrm{e}}^{(\mathrm{i})}\}$, and the cumulative angles to the midpoints of the arms $\{\theta_{\mathrm{m}}^{(\mathrm{i})}\}$. In addition, we use statistical methods to investigate possible correlations between parameters pertaining to the three individual arms of any given triskelion, e.g., to determine whether the apparent length of a triskelion arm is

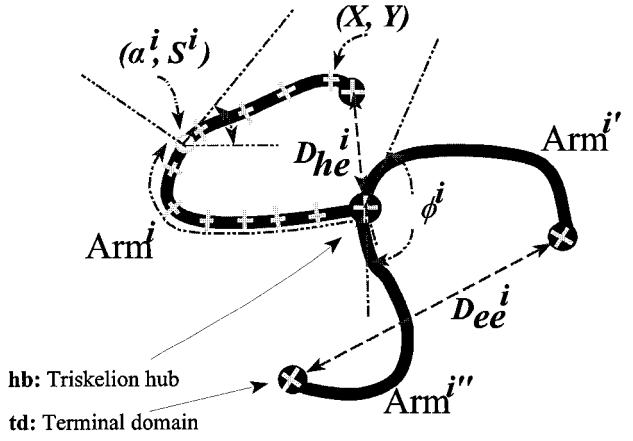

FIGURE 2 The notation adopted in this work. The quantities $S^{(i)}(s)$ and $\alpha^{(i)}(s)$ are, respectively, the apparent contour length and tangential angle of the ith arm at position s (the latter being measured along the amino acid backbone of the heavy chain), $\phi^{(i)}$ is the hub angle opposite the ith arm, $D_{he}^{(i)}$ is the linear distance between the hub and the center of the terminal domain of the ith arm, and $D_{ee}^{(i)}$ is the linear distance between the terminal domains of the apposing arms (i.e., between arms i' and i''). The latter notation is easy to comprehend if one recognizes that "h" stands for "hub," and "e" signifies "end" (at the terminal domain).

correlated with the total bending angle of that arm and/or with the lengths of other arms located within the same triskelion. In this way, we infer elements of a structural probability density specifying the likelihood of a triskelial shape profile when visualized by electron microscopy on a nanometer length scale.

ANALYSIS AND RESULTS

We find that the projected (two-dimensional) electron micrographic images of triskelions can be adequately described in terms of the following master probability density function,

$$\mathcal{P}(\{\alpha^{(i)}(s), S^{(i)}(s)\}) = \mathcal{P}_{hub}(\phi^{(1)}, \phi^{(2)}, \phi^{(3)}) \prod_{i=1,2,3} \mathcal{P}_{Arm}(\theta^{(i)}(s), S^{(i)}(s)). \quad (1)$$

In this expression, the index $i = 1, 2, 3$ pertains to the individual arms, characterized by the nanoscopic degrees of freedom $\alpha^{(i)}(s)$ and $S^{(i)}(s)$, where the tangential angle $\alpha^{(i)}(s)$ and the apparent contour length $S^{(i)}(s)$ of the ith arm both are functions of the distance along the true arm-length position s (which is linked to the amino acid sequence of the heavy chain). The principal feature of Eq. 1 is that $\mathcal{P}_{hub}$ $(\phi^{(1)}, \phi^{(2)}, \phi^{(3)})$ and the $\mathcal{P}_{Arm}$ $(\theta^{(i)}(s), S^{(i)}(s))$ specify independent behaviors of the hub angles and each of the three arms. [Here, $\theta^{(i)}(s) \equiv (\alpha^{(i)}(s) - \alpha^{(i)}(0))$ measures the net bending of Arm$^{(i)}$, and the variable $\phi^{(i)}$ denotes the angle, at the hub, between the two arms other than Arm$^{(i)}$ (see Fig. 2).]

The validity of Eq. 1 depends on the following postulates: 1) that the three arms within a triskelion have identical properties but fluctuate independently of each other; 2) that the shape fluctuations of the arms are independent of the relative orientation of the arms about the hub; and 3) that there are no special global shape constraints, such as preferred fixed distances between three terminal domains.

Distributions of triskelion global parameters

To establish these properties, we obtained statistical descriptors for the parameters D_{he}, D_{ee}, L, ϕ, θ_e, and θ_m discussed at the end of the previous section (see also Fig. 2). For each parameter A we constructed the overall frequency distribution by including data for all 72 intact triskelions (i.e., 216 arms). With but one exception (the hub angles: see below), these distributions appear to fit normal distributions, viz.,

$$\mathcal{P}_n(A) \equiv \frac{1}{\sqrt{2\pi}\,\sigma(A)} \times \exp\left\{ -\frac{1}{2}\left[\frac{A - \mu(A)}{\sigma(A)}\right]^2 \right\}, \quad (2)$$

where the average (mean) value $\mu(A)$ and the standard deviation $\sigma(A)$ are defined as $\mu(A) = \Sigma_{i=1}^{3}\,\Sigma_{j=1}^{N} A^{(i,j)}/3N$ and $\sigma^2(A) = \Sigma_{i=1}^{3}\,\Sigma_{j=1}^{N}\,(A^{(i,j)} - \mu(A))^2/(3N - 1)$, respectively. To establish whether the individual arms in a triskelion behave independently of each other, we determined values pertaining to the various arm parameters $\{A_{sm}^{(j)}\}$, $\{A_{md}^{(j)}\}$, and $\{A_{lg}^{(j)}\}$, where the subscripts "sm," "md," and "lg" denote, respectively, the smallest, the medial, and the largest value among each triplet of global parameters noted for any given triskelion image. If Eq. 2 holds and if the arms fluctuate independently, then the uniquely formed group of subsets, $\{A_{sm}\}$, $\{A_{md}\}$, and $\{A_{lg}\}$, will be practically indistinguishable from bell-shaped normal curves having the following parameter values (see Appendix B)

$$\begin{aligned} \mu(A_{sm}) &= \mu(A) - 0.846 \cdot \sigma(A), \\ \sigma(A_{sm}) &= 0.748 \cdot \sigma(A); \\ \mu(A_{md}) &= \mu(A), \\ \sigma(A_{md}) &= 0.670 \cdot \sigma(A); \\ \mu(A_{lg}) &= \mu(A) + 0.846 \cdot \sigma(A), \\ \sigma(A_{lg}) &= 0.748 \cdot \sigma(A). \end{aligned} \quad (3)$$

As an example, the frequency distributions for the arm contour length, L, are shown in Fig. 3. The overall form of arm lengths is seen to be symmetric and appears to be close to a normal distribution. Moreover, the measured contributions from the medial and smallest values of arm lengths are in good agreement with the predictions of Eqs. 3. Similar investigations were made of D_{he}, D_{ee}, θ_e, and θ_m. Each quantity was found to be nearly normally distributed, and all

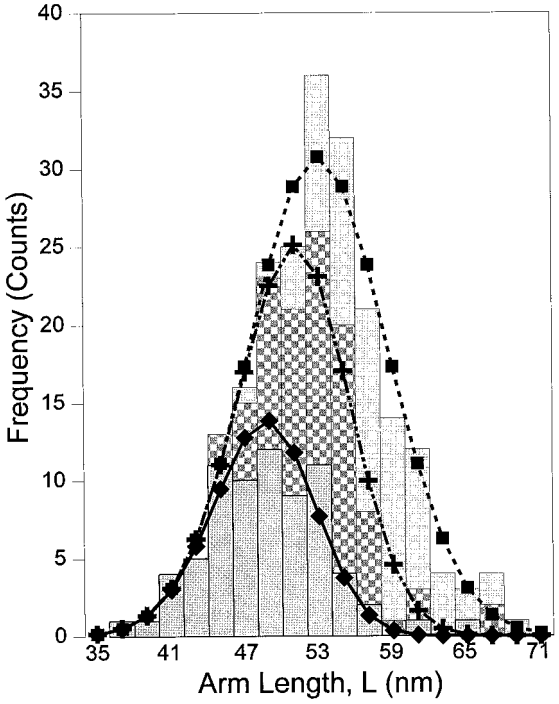

FIGURE 3 Frequency distribution of the apparent contour length, L, of the triskelion arm. The bars comprising the histogram are marked with distinctive patterns denoting contributions from subsets containing, respectively, the smallest (gray shading), the medial (lighter, cross-hatched pattern), and the largest (light, square grid pattern) values of every triplet of arm lengths for each of the 72 triskelion images. The curve defined by square symbols is a fit to a normal distribution (see Eq. 2), with measured values of the average (μ) and standard deviation (σ) for *all* arms pooled together. The diamond-marked curve is a normal distribution fit for the smallest subset, with theoretical values of $\mu(L_{sm})$ and $\sigma(L_{sm})$ calculated from Eqs. 3. The curve indicated by a "plus" sign is a fit to the sum of a pair of expected normal distributions, one being the distribution for the subset of smallest values and the other the subset of medial values, also calculated according to Eqs. 3. Our estimated average length, $\mu(L) = 53.5$ nm (see Table), is slightly greater than the value of 51.6 nm inferred by Kocsis et al. (1991) from a larger data set that included incomplete triskelia, but is almost identical to their most probable value of 53.3 nm.

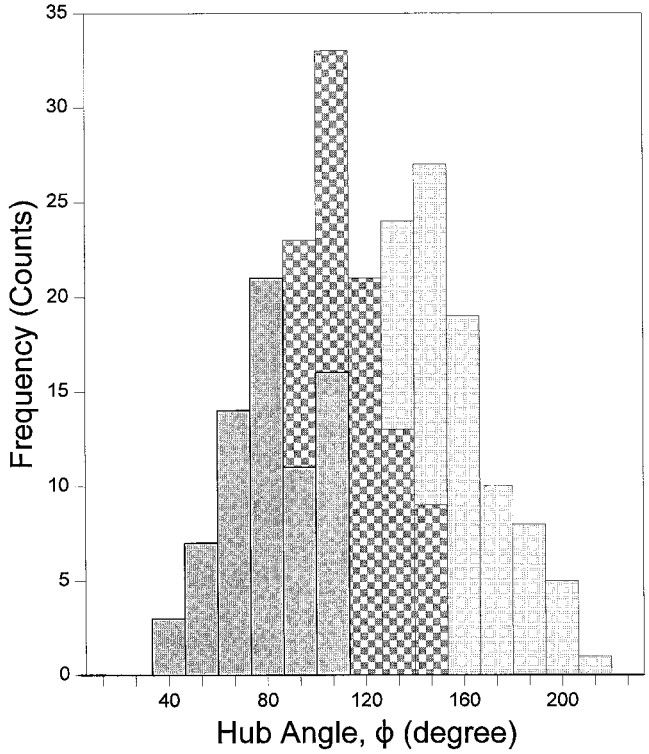

FIGURE 4 The frequency distributions (see caption to Fig. 3) of the hub angles, ϕ. As expected, the subset frequency distributions in this case do *not* fit bell-shaped, normal curves (see text).

indicate the independence and equivalence properties implied by Eqs. 3. The only variables that are not normally and independently distributed are the hub angles $\{\phi^{(i)}\}$, which is expected because the projected hub angles must obey the simple constraint $\Sigma_{i=1,2,3}\ \phi^{(i)} = 360°$. We note that the wide distribution of $\{\phi^{(i)}\}$ (see Fig. 4) signifies considerable flexibility of the arms near the central hub. In sum, though, distributions of the type shown in Fig. 3 and the statistical measures given in Table 1 support the notion that the arms are equivalent and fluctuate independently.

Correlations in global shape fluctuations

The possible linkage between pairs of arm variables $\{A^{(i)}\}$ and $\{B^{(i)}\}$ (where, e.g., $A^{(i)} = L^{(i)}$, $B^{(i)} = \phi^{(i)}$) can be investigated according to conventional correlation coefficients, $\{\rho(A, B)\}$, whose definition is given by Eq. C1 in Appendix C. When applied to our data, we obtain the values $\{\rho(\phi, A)\}$ shown in Table 2 where, for example, $\rho(\phi, L)$ tests the correlation between the arm length L and the opposite hub angle ϕ. Because we have images of only 216 arms, and thus only 144 independent measures of ϕ, all these values essentially are indistinguishable from zero at a confidence level of 95% (for 144 samples, the limits are $|\rho(A, B)| \leq 0.16$, see Appendix C). Moreover, the corresponding scatterplots for all five pairs, (ϕ, L), (ϕ, θ_e), (ϕ, θ_m), (ϕ, D_{he}), and (ϕ, D_{ee}), do not indicate any recognizable pattern (data not shown). Hence, the hub degrees of freedom as measured by ϕ seem to be totally independent of the arm degrees of freedom, $\{L, \theta_e, \theta_m, D_{he}, D_{ee}\}$. This independence supports the separation of the hub and arm terms in the master probability density function (see Eq. 1), and implies that the hubs do not have any significant role in controlling arm shape change.

Additional support for the independence and equivalence of arm fluctuations is provided by calculating a novel tri-correlation coefficient ρ_s, which also is defined in Appendix C. This coefficient tests correlations among three variables, $A1$, $A2$, and $A3$, having identical distributions. If the subsets $\{A1\}$, $\{A2\}$, and $\{A3\}$ are formed from independent sampling, then $\rho_s\ (A) \simeq 0$; however, if $A1$, $A2$, and $A3$ are strictly correlated by the constraint $A1 + A2 + A3 = \text{const.}$,

TABLE 1 Comparisons between measurements and predictions

Characteristic Quantities	Average value (μ) ± Standard deviation (σ) Overall (all data)	Smallest (or Shortest)	Medial	Largest (or Longest)
L (nm)				
measurement	53.6 ± 5.7	49.2 ± 4.9	53.4 ± 4.1	58.0 ± 4.1
theory	—	48.7 ± 4.3	53.6 ± 3.8	58.3 ± 5.4
D_{he} (nm)				
measurement	29.7 ± 7.2	23.7 ± 6.0	29.9 ± 4.3	35.4 ± 5.7
theory	—	23.6 ± 5.4	29.7 ± 4.8	35.8 ± 5.4
D_{ee} (nm)				
measurement	49.5 ± 11.3	39.8 ± 8.6	51.0 ± 8.2	57.6 ± 8.9
theory	—	39.9 ± 8.4	59.5 ± 7.6	59.0 ± 8.4
θ_e (degree)				
measurement	152 ± 58	100 ± 50	158 ± 37	198 ± 38
theory	—	103 ± 44	152 ± 40	201 ± 44
θ_m (degree)				
measurement	73 ± 40	38 ± 31	71 ± 26	109 ± 26
theory	—	38 ± 30	73 ± 27	107 ± 30
ϕ (degree)				
measurement	120 ± 37	82 ± 20	118 ± 16	161 ± 21
theory	—	Non-normal	Non-normal	Non-normal

Parameters of frequency distributions of global quantities such as the apparent arm length L and total arm bending angle θ_e that characterize the two-dimensional, nanoscopic shape fluctuations of triskelions (see Fig. 2 and related text). Measured mean values, $\mu(A)$, and standard deviations, $\sigma(A)$, for all arms pooled together, and for the smallest, medial, and largest subsets (see text) are compared with values inferred from Eqs. 3. [For Gaussian (normal) distributions, the standard errors of the reported mean values are related to the standard deviations by $\sigma/\sqrt{N-1}$, where $N = 216$ is our sample size.]

then $\rho_s(A) = -1$. Values of ρ_s for arm descriptors of interest are given on the second line of Table 2. Because there are only 72 triskelions, these numbers are considered to be not statistically different from zero at a 95% confidence limit if $|\rho_s| \leq 0.27$ (see Appendix C). Tricorrelation coefficients pertaining to arm bending, viz., $\rho_s(\theta_e)$, $\rho_s(\theta_m)$, and $\rho_s(D_{he})$, lie well within this range. Note, however, that $\rho_s(L)$ and $\rho_s(D_{ee})$ have slightly higher values, which may indicate that, when samples are prepared for electron microscopy, the hubs of some triskelia sit slightly above the mica surface due to an intrinsic triskelial pucker (Kirchhausen et al., 1986).

Taken together, the behaviors of these correlation relations further support the view that the three arms of triskelions fluctuate independently and that they have essentially identical physical properties. The probability density function given by Eq. 1 seems to apply in a self-consistent manner.

TABLE 2 Correlation coefficients, $\rho(\phi, A)$ and $\rho_s(A)$, as computed by Eqs. C1 and C2 for the various global-shape parameters

A	θ_m	θ_e	L	D_{ee}	D_{he}	ϕ
$\rho(\phi,A)$	−0.17	−0.10	0.06	0.05	0.15	—
$\rho_s(A)$	−0.18	−0.07	0.29	0.17	0.34	−1*

Fluctuations about the mean triskelion shape

We also determined the average shape of a triskelion arm and the fluctuations about the mean contour. Such data are of central importance to our subsequent analysis of arm energetics. From the 72 intact triskelions, we examined 216 triskelion arms by considering each to be an equivalent member of an ensemble and calculated the mean and standard deviation of the local curvature (i.e., the gradient of the tangential angle as one moves along a triskelion arm; see Eq. A4). Results are presented in Fig. 5, where the lower points (*circles*) represent the mean value of curvature, $\bar{C}(s)$, as a function of intrinsic position along the triskelion arm, s (the distance from the hub when scaled to the apparent arm length). The upper points (*triangles*) show the corresponding values of the standard deviation in the local curvature, $\sigma(C(s))$ (see Appendix A). Two important points should be noted. First, the arms, on average, are almost continuously curved, and there are no sharp bends in the structure. Second, except for the positions near the hub and terminal domains, the values of $\sigma(C(s))$ vary by $<20\%$, indicating that the bending rigidity is approximately constant along the entire arm. The fact that the standard deviations of the fluctuations are large signifies that the arm shapes are quite variable (see Fig. 1).

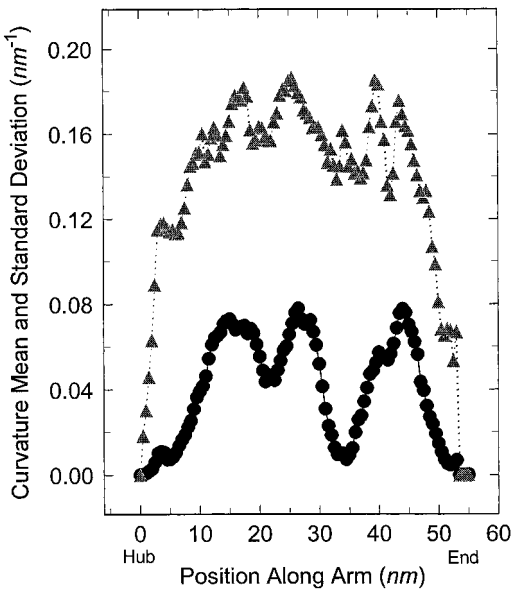

FIGURE 5 Mean curvature, $\bar{C}(s)$, (*circles, bottom curve*) and standard deviation, $\sigma(C(s))$, (*triangles, top curve*) along clathrin arms, as a function of the distance along the molecular backbone, s, from the hub. Note that the scale on the ordinate is identical for both $\bar{C}(s)$ and $\sigma(C)$.

Bending rigidity of individual clathrin arms

Quantitative calculations of the bending rigidity of the arms is simplified by the fact that the arms are approximately uniformly flexible along their length. The bending energy per unit length, $\partial U/\partial s$, associated with the distortion, $C(s) - C_0(s)$, of a thin wirelike body can be written as (Landau and Lifshitz, 1959; Gittes et al., 1993)

$$\frac{\partial U}{\partial s} = \frac{1}{2} EI\Big(C(s) - C_0(s)\Big)^2 + \ldots . \tag{4}$$

Here, $C_0(s)$ is the curvature of the arm in the relaxed conformation (assumed to be equal to $\bar{C}(s)$), and the quantity EI is the average flexural rigidity. Applicability of Eq. 4 requires that the local radius of curvature be much larger than the thickness of the clathrin arm and that, on a nanoscopic length scale, its material properties be isotropic; we also assume that, at least to first-order, length-stretching and/or compression is independent of arm bending, so the true position along the arm, s, simply is proportional to its apparent contour location S. Thus, the bending energy of an arm may be written for any particular configuration as

$$U_{\text{bend}} \approx \frac{1}{2} EI \int_0^{s_{\text{td}}} [C(s) - C_0(s)]^2 \, \mathrm{d}s, \tag{5}$$

where s_{td} denotes the position of the terminal domain.

As remarked upon below in the Summary and Discussion, we assume that, to good approximation, triskelion conformations along the flat mica substrates are not perturbed by triskelion–mica interactions. It then follows from the Boltzmann relation for molecular systems interacting with a heat bath (Reif, 1965) that the probability density for arm bending may be expressed, according to Eq. 5, as

$$\mathcal{P}_{\text{arm}} \sim \exp\left(-(k_{\text{B}}T)^{-1} \int_0^{s_{\text{td}}} \left\{\frac{1}{2} \cdot EI \cdot [C(s) - C_0(s)]^2\right\} \mathrm{d}s\right), \tag{6}$$

where k_{B} is Boltzmann's constant and T is the absolute temperature. When Eq. 6 is used along with a normal mode decomposition of triskelion shape, variances in mode amplitudes $\{\langle (a_{\text{n}} - a_{\text{n}}^0)^2 \rangle\}$ can be linked to the flexural rigidity as

$$\langle (a_{\text{n}} - a_{\text{n}}^0)^2 \rangle \approx \frac{k_{\text{B}}T}{EI}\left(\frac{L}{n\pi}\right)^2 + SV, \tag{7}$$

where L is the intrinsic (average) length of a triskelial arm and SV is a constant (see Appendix D). In Fig. 6, we show a two parameter least squares fit of Eq. 7 to computed mode amplitude fluctuations, from which we obtain the value $EI_{\text{arm}} \simeq 35\ k_{\text{B}}T$·nm (from the slope) and $SV \simeq 1.7$ nm (as the background).

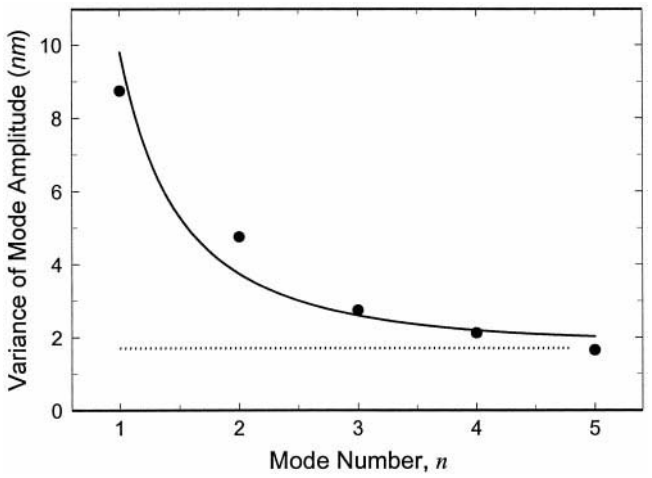

FIGURE 6 Estimation of EI from the variance of the amplitudes $\langle (a_{\text{n}} - a_{\text{n}}^0)^2 \rangle$ of the five leading modes. The fitted curve (Eq. 7) depicts the expected $1/n^2$ behavior in the presence of noise due to uncertainty in resolving the electron microscope images plus uncertainty arising from the spline fits (*dotted line*).

Comparative bending energy

Because portions of four arms overlap when triskelions assemble into a lattice (Crowther and Pearse, 1981), the flexural rigidity, EI_{bond}, of a lattice bond (an edge between two vertices, see Fig. 7) is higher than that of a single arm, EI_{arm}. For isotropic elastic substances, the flexural rigidity can be expressed as the product of the Young's Modulus of the material, E, and the moment of inertia, I, of the structure, i.e.,

$$EI = E \cdot I, \tag{8}$$

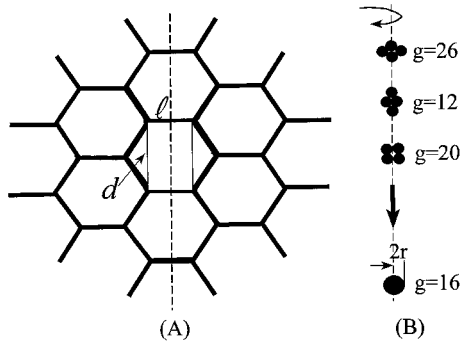

FIGURE 7 (*A*) Idealized, flat hexagonal clathrin lattice overlaying a hypothetical membrane. Bending is assumed to occur about the axis defined by the dashed line. The bending energy of the elemental membrane area (designated by the shaded region) is to be compared with the energy needed to bend a "bond" between two vertices (e.g., the edge marked l in the figure). (*B*) Possible cross-sections of the bonds (composed of four triskelial arms) and their corresponding g values (see Eq. 9), for bending in the direction indicated by the curved arrow.

where $I = \iint_{\text{cross section}} y^2\, dA$ (e.g., $I = \pi r^4/4$ for a circular rod). Suppose we adopt the current structural model of clathrin cages (Ybe et al., 1999) and presume that the axes of the individual overlapping arms (all having the same cross sections) are equidistant from the center of mass of the composite structure. By assuming that the mass of the composite is uniformly distributed within a cross sectional area whose radius is twice that of an individual arm, we infer the result

$$EI_{\text{bond}} = gEI_{\text{arm}}, \tag{9}$$

where $g = 16$. If, however, the arms are asymmetrically arranged, then g will differ from this value and depend on the plane of bending. In Fig. 7, we show some examples, calculated according to the integral appearing after Eq. 8. For reasonable geometric cross sections, we find values of g lying between 12 and 26. Because the arms are likely to be twisted about each other (Ybe et al., 1999), a weighted average of these values might be appropriate so the value $EI_{\text{bond}} \simeq 16EI_{\text{arm}}$ probably is a good choice (see also Summary and Discussion below).

Consider that the clathrin triskelions assemble to form the regular planar structure shown in Fig. 7. Let us now compare the energy necessary to bend a patch of membrane (the shaded area in Fig. 7) with the energy needed to bend an equivalent clathrin net. Bending is assumed to occur about the axis defined by the dotted line. Upon referring to Eq. 5, we see that the energy associated with the distortion of a lattice bond is

$$U_{\text{bond}} = \frac{1}{2} EI_{\text{bond}} \int_0^{\ell} \left(\frac{1}{R_1}\right)^2 dx, \tag{10}$$

where $R_1 \equiv 1/C_1$ is the radius of curvature, assumed to be constant over the entire length of the bond. Similarly, the energy required to bend the elemental equivalent membrane patch can be estimated by

$$\begin{aligned} U_{\text{mb}} &= \frac{1}{2} \kappa_{\text{mb}} \int_{\text{area}} \left(\frac{1}{R_1}\right)^2 dA \\ &= \frac{1}{2} \kappa_{\text{mb}} \cdot d \int_0^{\ell} \left(\frac{1}{R_1}\right)^2 dx \\ &\equiv \frac{1}{2} EI_{\text{memb}} \int_0^{1} \left(\frac{1}{R_1}\right)^2 dx, \end{aligned} \tag{11}$$

where we have assumed the usual expression for bending energy per unit area for a cylindrical membrane (Helfrich, 1973), viz., $u \approx \frac{1}{2}\, \kappa_{\text{mb}}\, (1/R_1)^2$. Here, the equivalent bending rigidity of the membrane is defined, in terms of bending modulus κ_{mb} and lateral distance d, as $EI_{\text{memb}} = \kappa_{\text{mb}} \cdot d$. From Fig. 7, the distance d is seen to be $d = \sqrt{3}l$, yielding, for a clathrin lattice, the value $d \simeq 32$ nm (Vigers et al., 1986). Thus, using a typical value of $\kappa_{\text{mb}} \approx 10$–$30 k_{\text{B}}T$ for phospholipid bilayers (see Zhelev et al., 1994; Seifert and Lipowsky, 1995), we find $EI_{\text{memb}} \approx 320$–$960\ k_{\text{B}}T$·nm. This number is to be compared with EI_{bond} which, when using our previously derived estimate ($EI_{\text{arm}} \simeq 35\ k_{\text{B}}T$·nm), is $EI_{\text{bond}} \simeq 16 \cdot EI_{\text{arm}} \simeq 560\ k_{\text{B}}T$·nm.

SUMMARY AND DISCUSSION

A central focus of this work has been to examine whether clathrin plays a significant mechanical role in endocytic vesicle formation. We analyzed shape fluctuations in electron microscope images of individual triskelions and used expressions based on equilibrium statistical physics to estimate the mean bending rigidity of a clathrin arm of a typical triskelion. We then compared the energy needed to bend a region of clathrin lattice with that necessary to bend an equivalent membrane patch, and inferred that the energies are comparable. Although the preparation of the electron micrographs may introduce structural features into the triskelial images that are not found in a simple, equilibrium aqueous environment, we believe that our investigation provides a valid order-of-magnitude estimate of the mechanical role of the protein coats in clathrin-coated vesicles.

This study has several consequences. First, the statistical analysis in this paper provides significant information concerning the global structural properties of triskelions—viz., the independence, equivalence, and uniformity of flexibility of the arms. One implication is that the large and uniform flexibility of the arms allows for assembly of baskets and nets of widely different structure. Also, although the light clathrin chains that are bound to the triskelion arms are known to comprise at least two classes, the arm equivalence noted in our fluctuation analyses supports the thesis that light chains, at most, play only a small intratriskelion structural role. Moreover, the lack of any evidence that information about arm extensions are transmitted across the hub region suggests that mechanical models of clathrin basket formation probably can be posited without concern for hub distortions. Finally—of greatest significance—it appears that the energy needed to bend a clathrin net is of the same order of magnitude as the energy expended to bend an equivalent membrane patch. This result strongly suggests that a major role for clathrin is to assist in the formation of endocytic and intracellular vesicles by changing the mechanical properties of the composite membrane. It now is clear that, due to its intrinsic curvature and relatively high rigidity, the basket-like clathrin coat can stabilize vesicles of ~1000-Å radius and thereby play a significant energetic role during coated vesicle formation.

Potential errors in the analysis most likely are linked to intrinsic artifacts arising during preparation of specimens for electron microscopy. But, as explained in this and the

following two paragraphs, these undoubtedly would lead to an underestimation of the mechanical rigidity of the lattice, so our basic findings are unaffected. We worry most that extraneous bends in the triskelial arms can be introduced during placement of the triskelia onto the microscope grid. For example, the arms of a triskelion might interact with the substrate before the hub region attaches, causing them to buckle as the triskelion settles onto the mica surface; also, imperfections in the mica surfaces, or peculiarities of the interactions of the surfaces with the triskelia, might induce spurious bends. However, were these to happen, the triskelions would appear to be more flexible (i.e., less rigid) than they really are. The incumbent shape changes would add to the intrinsic, thermally induced fluctuations, leading to an underestimation of the arm rigidity. It is hard to envision how sample preparation could have an opposite effect, i.e., the straightening of arms and resultant overestimate of triskelial rigidity. We also note that, although heavy-metal shadowing of the triskelia tends to obscure fine details, our analysis is based on low-order modes (see Fig. 6), which are relatively unaffected.

Comparison of the persistence length measured from negative stained carbon-film electron micrographs of actin filaments with that determined by light microscopy indicated that negative-stained electron microscopy indeed provides a good estimate of the flexibility of the filaments (Orlova and Egelman, 1993). Similar inferences have been drawn regarding the fidelity of rotary shadowed DNA absorbed to carbon films (Griffith et al., 1986), although later studies of the absorption of DNA molecules onto mica surfaces suggest that the resulting images depend on sample deposition conditions (Rivetti, et al., 1996). However, in the latter investigation, DNA samples were prepared by drying simple aqueous solutions, whereas the triskelion samples examined in this study were deposited to the mica surfaces by glycerol nebulization. The viscosity of the glycerol/water mixture used in the nebulization process increases very sharply as a specimen is dried, and the resultant glassy solidification of the sample probably tends to preserve the natural distribution of triskelion shape conformations.

Additional evidence that the flexibility of clathrin noted in these micrographs is an intrinsic property of the triskelions is inferred from the fact that, when prepared in a similar way, samples of thin elongated molecules such as the filamentous hemagglutinin of *Bordetella pertussis* appear straight and rigid (Kocsis et al., 1991). Moreover, our investigations mainly concern fluctuations within the surface plane of the mica, which is very smooth and should provide little in-plane force modulation on a nanometer length scale. Indication that the sample preparation is relatively benign follows from studies of possible correlations between descriptors for the three arms of the same triskelions: because the shapes of the arms within individual triskelions appear to be independent, one can rule out the possibility that the observed fluctuations are significantly affected by localized features of the mica surfaces or such factors as solvent flows during sample deposition. For these reasons we believe that, at least to a first approximation, complications due to interactions between triskelions and the mica surfaces can be ignored in our analysis.

Another uncertainty in our analysis is the estimate of the flexural rigidity for a link in the clathrin lattice, EI_{bond}, which may be greater than the value $16EI_{arm}$ obtained by assuming that the four overlapping arms lie symmetrically about each other. If the arms were to lie adjacent to each other in a plane, and if the bending were to occur in that plane, the effective flexural rigidity could be considerably higher. However, there is no evidence that such an asymmetric structure exists; to the contrary, recent high-resolution electron microscopy studies indicate that the arms form a twisted bundle of essentially symmetric cross-section when incorporated into clathrin cages (Smith et al., 1998; Ybe et al., 1999). Again, though, even if we have underestimated EI_{arm}, our qualitative conclusion about the relative importance of the clathrin lattice is unaffected.

In vivo conditions may be yet more favorable to the mechanical role played by the clathrin relative to that of the underlying membrane. Thermodynamic analysis (Nossal, 1998) of the sizes of clathrin baskets assembled in the presence of "assembly polypeptides" (Zaremba and Keen, 1983) indicates that certain accessory coat proteins, which are present on the surfaces of endocytic vesicles, increase the rigidity of the clathrin lattice. Also, our estimate of the membrane flexural rigidity, EI_{memb}, may be somewhat high, due to the fact that the underlying membrane parameter κ_{mb}, is somewhat uncertain. Although the values of overall membrane rigidity used in our analysis probably are of the correct order of magnitude, it is likely that membrane regions that bud off to form vesicles have properties that differ from the average; e.g., biochemical reactions might have the effect of lowering κ_{mb} by changing the local lipid composition or properties of the submembraneous cytoskeleton. Modification of the relative rigidities of plasma membrane and clathrin lattice could be a regulatory mechanism for vesicle budding at a cell surface. The dependence of the g factor on triskelion arm packing geometry (see Eq. 9 and Fig. 7), with its incumbent effect on EI_{bond}, also implies possibilities for intracellular control of clathrin vesicle formation.

APPENDIX A

CHARACTERIZATION OF ARM SHAPES

From the digitized shape data provided for each triskelion (see Fig. 1), we generated a set of smooth natural cubic spline functions by fitting each contiguous, overlapping group of four nodes by a cubic equation (Press, et al., 1988). From these, we obtained the coordinate sets $\{X^{(i,j)}(t)\ Y^{(i,j)}(t)\}$, where $t = [0, 1, \ldots, t_{td} = 100]$ is an index that increases sequentially from 0 at the triskelion hub to t_{td} at the center of the terminal domain, and (i, j)

indicates the ith arm of the jth triskelion. As illustrated in Fig. 1, the spacing between the nodal points of the primary data sets is not uniform, but tends to accentuate regions of high curvature: fewer nodal points were used to describe those portions of a triskelion that appeared to be straight (Kocsis et al., 1991). To preserve the weight given to regions of high curvature, the newly generated intermediate points $\{t\}$ were taken in identical numbers between each neighboring pair of original digitized nodal points. The value of $t_{td} = 100$ provides meaningful numerical accuracy. Because possible error in the coordinates of the original nodes is of the order of one-fifth the spacing between nearest nodes (Kocsis et al., 1991), a finer mesh size (i.e., greater number of $\{t\}$) did not seem to be warranted.

To describe the shapes of the arms, we computed the arm contour lengths $S^{(i,j)}(t)$ and arm tangential angles $\alpha^{(i,j)}(t)$ according to the following relations:

$$S(t) = \sum_{t'=1}^{t} \sqrt{\left(\frac{dY(t')}{dt'}\right)^2 + \left(\frac{dX(t')}{dt'}\right)^2} \tag{A1}$$

(with $S(0) = 0.0$ Å) and

$$\alpha(t) = \tan^{-1}\left(\frac{dY(t)/dt}{dX(t)/dt}\right). \tag{A2}$$

These functions were evaluated, for each triskelion arm, at all extrapolated nodal points $\{t = 0, 1, 2, \ldots, t_{td}\}$ pertaining to that arm. We allowed $\alpha(t)$ to range from 0° to 360°, and were careful to properly invert the tan-functions. The values of $\{S^{(i,j)}(t), \alpha^{(i,j)}(t)\}$ provide a description of the contour of a given triskelion arm that is equivalent to the points $\{X^{(i,j)}(t), Y^{(i,j)}(t)\}$.

All global shape quantities were calculated from these equivalent data sets. For example, the apparent length of each arm was obtained as $L = S(t = t_{td}) + R_{td}$, where $R_{td} = 36$ Å is the average radius of the triskelion terminal domains (measured by Kocsis et al., 1991). The hub angles, $\phi^{(i,j)}$ (see Fig. 2), were determined from the difference in the initial directions of the two other arms, the latter being $\alpha^{(i',j)}(0)$ and $\alpha^{(i'',j)}(0)$. The total cumulative hub-to-terminal angle was computed as $\theta_e = \alpha(t_{td}) - \alpha(0)$. We also calculated the cumulative angle to a point midway along the arm according to $\theta_m = \text{linterp}\,(\alpha(t)|S(t) = L/2) - \alpha(0)$, where linterp($\alpha$) denotes a simple linear interpolation between values of α at those nodal points lying to both sides of the midpoint $S = L/2$ when the apparent length of the arm is L. The hub-to-terminal distances D_{he} and terminal domain–terminal domain distance D_{ee} were calculated according to

$$D_{he}^{(i,j)} = \sqrt{(X_{hb}^{(j)} - X_{td}^{(i,j)})^2 + (Y_{hb}^{(j)} - Y_{td}^{(i,j)})^2};$$
$$i = 1, 2, 3; \quad j = 1, 2, \ldots, 72$$

and

$$D_{ee}^{(i,j)} = \sqrt{(X_{td}^{(i',j)} - X_{td}^{(i'',j)})^2 + (Y_{td}^{(i',j)} - Y_{td}^{(i'',j)})^2},$$
$$\text{where} \quad i = 1, 2, 3 \quad \text{and} \quad i' \neq i'' \neq i.$$

To examine the bending profiles and rigidity of triskelion arms, we computed the true position, s, along the arms by scaling the observed arm length of each triskelion according to the linear relationship

$$s^{(i,j)}(t) = S^{(i,j)}(t)\left[\frac{\mu(L) - R_{td}}{S^{(i,j)}(t_{td})}\right], \quad t = 0, \ldots, t_{td} = 100. \tag{A3}$$

To determine the corresponding $\alpha^{(i,j)}$, we then inverted Eq. A3 to identify the interpolated value $t^{(i,j)}$ (not necessarily an integer) corresponding to a given value s. Associated with these $\{t^{(i,j)}\}$ are the derived values $\{\alpha^{(i,j)}(s)\}$, calculated from Eq. A2 by using the spline functions $\{X^{(i,j)}(t), Y^{(i,j)}(t)\}$. The curvatures $\{C^{(i,j)}\}$ then were calculated via

$$C^{(i,j)}(s) = \frac{\Delta\alpha^{(i,j)}(t^{(i,j)}(s))}{\Delta s}, \tag{A4}$$

$$s = 0, \frac{\mu(L)}{100}, \frac{2\mu(L)}{100}, \ldots, \mu(L),$$

where $\Delta\alpha/\Delta s$ represents a finite difference. For each triskelion, we separately calculated $C^{(i,j)}(s)$ ($i = 1, 2, 3$; $j = 1, 2, \ldots, 72$) at each of the expanded internodal coordinate points. We also calculated the mean value of the curvature, $\bar{C}(s) \equiv \sum_{i,j} C^{(i,j)}(s)/216$, and the standard deviation,

$$\sigma(C(s)) \equiv \left[\frac{\sum_{i,j} (C^{(i,j)}(s) - \bar{C}(s))^2}{215}\right]^{1/2}.$$

The spline fits and several other data-reduction steps were carried out on a desktop personal computer, primarily using the MATHCAD software package (MathSoft, Cambridge, MA). The codes developed during this work are available upon request from Dr. A. J. Jin.

APPENDIX B

RELATIONSHIPS BETWEEN SUBSET DISTRIBUTIONS

As already mentioned, we measured various global parameters $\{A^{(i,j)}\}$, where $A^{(\cdot)}$ represents a quantity such as arm length $L^{(\cdot)}$, the index $i(= 1, 2, 3)$ pertains to a particular arm within a given triskelion, and $j(= 1, \ldots, N)$ denotes different triskelions. These j triplet values allowed us to examine, in addition to the overall distribution of the complete set $\{A^{(i,j)}\}$, the three subset distributions $\{A_{sm}^{(j)}\}$, $\{A_{md}^{(j)}\}$, and $\{A_{lg}^{(j)}\}$, which are uniquely defined and consist, respectively, of the smallest, the medial, and the largest value within each triplet. We now provide a proof of Eqs. 3, which have been used to infer the independence of arm fluctuations within individual triskelions.

Suppose, for any set of N triskelion images, we arbitrarily form the subsets $\{A^{(1,j)}\}$, $\{A^{(2,j)}\}$, and $\{A^{(3,j)}\}$, where each subset contains the value of A for one, and only one, arm of each triskelion. If the arms of particular triskelions fluctuate independently and equivalently, then the distributions of the subsets will be identical to that of the entire collection of $\{A\}$ values $\mathcal{P}(A)$, and $\mathcal{P}(A^{(1)}, \mathcal{P}A^{(2)}, \mathcal{P}A^{(3)}) = \mathcal{P}(A^{(1)}) \cdot \mathcal{P}(A^{(2)}) \cdot \mathcal{P}(A^{(3)})$. It thus follows that

$$\mathcal{P}_{sm}(A) \propto 3\mathcal{P}(A) \cdot \left[\int_A^{\infty} \mathcal{P}(A')\, dA'\right]^2, \tag{B1}$$

because, by specifying that the smallest value $A^{(i)}$ is equal to A, one indicates that the values pertaining to the other arms are greater than A. The factor 3 arises because each of the three subsets contributes in the same way to the defined group containing the smallest values. Similarly, one finds

$$\mathcal{P}_{md}(A) \propto 6\mathcal{P}(A) \cdot \left[\int_{-\infty}^{A} \mathcal{P}(A')\, dA' \cdot \int_A^{\infty} \mathcal{P}(A')\, dA'\right] \tag{B2}$$

(in this case, there being six ways to sample the ensemble), and

$$\mathcal{P}_{lg}(A) \propto 3\mathcal{P}(A) \cdot \left[\int_{-\infty}^{A} \mathcal{P}(A')\, dA'\right]^2. \quad \text{(B3)}$$

If $\mathcal{P}$(A) approximates the normal distribution given in Eq. 2, viz., $\mathcal{P}_n(A; \mu(A), \sigma(A))$, then $\mathcal{P}_{sm}(A)$, $\mathcal{P}_{md}(A)$, and $\mathcal{P}_{lg}(A)$ are themselves approximately bell-shaped. To demonstrate this, we first perform a set of variable transformations in Eqs. B1–B3. These yield the relationships (1) $\mathcal{P}_{sm}(A \equiv \mu(A) - x \cdot \sigma(A)) = \mathcal{P}_{lg}(A' \equiv \mu(A) + x \cdot \sigma(A)) = f_1(x)$ and (2) $\mathcal{P}_{md}(A \equiv \mu(A) + x \cdot \sigma(A)) = f_2(x)$, where

$$f_1(x) \equiv \frac{3}{(2\pi)^{3/2}} e^{-x^2/2}\left[\int_{-\infty}^{x} e^{-t^2/2}\, dt\right]^2 \quad \text{(B4)}$$

and

$$f_2(x) \equiv \frac{3}{(2\pi)} e^{-x^2/2}\left[2\int_{-\infty}^{x} e^{-t^2/2}\, dt \cdot \left(1 - \frac{1}{(2\pi)^{1/2}}\int_{-\infty}^{x} e^{-t^2/2}\, dt\right)\right]. \quad \text{(B5)}$$

Numerical fitting by MATHCAD (MathSoft) indicates that $f_1(x)$ and $f_2(x)$ are virtually indistinguishable from the normal density functions $f_1^{norm}(x) = (1/\sqrt{2\pi}\sigma_1)\exp[-(x-\mu_1)^2/2\sigma_1^2]$ and $f_2^{norm}(x) = (1/\sqrt{2\pi}\sigma_2)\exp[-(x-\mu_2)^2/2\sigma_2^2]$ when μ_1, σ_1, μ_2, σ_2 have the values

$$\mu_1 \equiv \int_{-\infty}^{\infty} x f_1(x)\, dx \simeq 0.846, \quad \text{(B6a)}$$

$$\sigma_1 \equiv \left[\int_{-\infty}^{\infty} x^2 f_1(x)\, dx\right]^{1/2} \simeq 0.748, \quad \text{(B6b)}$$

$$\mu_2 \equiv \int_{-\infty}^{\infty} x f_2(x)\, dx = 0.0, \quad \text{(B6c)}$$

and

$$\sigma_2 \equiv \left[\int_{-\infty}^{\infty} x^2 f_2(x)\, dx\right]^{1/2} \simeq 0.670. \quad \text{(B6d)}$$

Several statistical tests can be used to verify the concordance of the distributions given by Eqs. B4–B6 with their respective normal distributions. We here adopted the approach of Kolmogorov–Smirnov (Sachs, 1978). This test depends on the "statistic D," which compares the maximum absolute difference between two cumulative distributions and is used to estimate the minimum sample number that is required to distinguish between distributions at a given confidence level α. It is a straightforward task to show that the maximum absolute cumulative differences $|f_1(x) - f_1^{norm}(x)|$ and $|f_2(x) - f_2^{norm}(x)|$ are approximately 0.015 and 0.001. Taking $\alpha = 0.05$, the Kolmogorov–Smirnov test suggests that at least 8000 triskelion images would be required to distinguish between $f_1(x)$ and $f_1^{norm}(x)$, whereas over 1.5 million samples would be necessary to distinguish between $f_2(x)$ and $f_2^{norm}(x)$. Consequently, the original subset distributions $\mathcal{P}_{sm}(A)$, $\mathcal{P}_{md}(A)$, and $\mathcal{P}_{lg}(A)$ also are indistinguishable from their respective normal distributions, with mean values and standard deviations given by

$$\begin{aligned}
\mu(A_{sm}) &= \mu(A) - \mu_1 \cdot \sigma(A),\\
\sigma(A_{sm}) &= \sigma_1 \cdot \sigma(A);\\
\mu(A_{md}) &= \mu(A) + \mu_2 \cdot \sigma(A),\\
\sigma(A_{md}) &= \sigma_2 \cdot \sigma(A);\\
\mu(A_{lg}) &= \mu(A) + \mu_1 \cdot \sigma(A),\\
\sigma(A_{lg}) &= \sigma_1 \cdot \sigma(A).
\end{aligned} \quad \text{(B7)}$$

By inserting the values for μ_1, μ_2, σ_1, and σ_2 given in Eqs. B6, one immediately obtains the relationships given in Eqs. 3 of the text.

APPENDIX C

STATISTICAL LIMITS OF CORRELATION COEFFICIENTS

The correlation coefficient $\rho(A, B)$ is defined as

$$\rho(A, B) \equiv \frac{\mu([A - \mu(A)][B - \mu(B)])}{\sigma(A)\sigma(B)}, \quad \text{(C1)}$$

where A, B are any pair of random variables and the functions $\mu(\cdot)$ and $\sigma(\cdot)$ are as defined previously, following Eq. 2. Correspondingly, we define a tricorrelation coefficient as

$$\rho_s(A) = \frac{\sum_{i=1}^{N}(A1^{(i)} + A2^{(i)} + A3^{(i)} - 3\mu(A))^2}{\sum_{i=1}^{3N}(A^{(i)} - \mu(A))^2} - 1. \quad \text{(C2)}$$

Here, N again is the number of triskelion arms in the data set, the quantities $A1$, $A2$, and $A3$ denote shape parameters for different arms of the same triskelion, and $\mu(A)$ is the mean value of the shape parameter for the entire data set. $\rho_s(A)$ is invariant under exchange of the elements within the triplets $\{A1, A2, A3\}$. The values of $\rho_s(A)$ can be used to determine relationships between $A1$, $A2$, and $A3$.

Because the numbers of samples that we have been able to analyze are rather small (216 triskelial arms; 144 independent angles where the arms join the hub; etc.), correlation coefficients obtained according to Eqs. C1 and C2 must be subjected to statistical analyses to assess their significance. We found, for example, that the conventional correlation coefficient $\rho(\phi, L)$ given by Eq. 4 has a value 0.06. With what probability is this value not notably different from zero, a value that signifies that ϕ and L are independent?

If $|\rho(A, B)|$ lies within values appropriate to a statistical confidence level (normally taken to be 95%), the variations of $\{A\}$ and $\{B\}$ probably are independent; if $|\rho(A, B)|$ lies outside this range, the variables probably are correlated (Sachs, 1978). The confidence levels of inferred values of $\rho(A, B)$, where A and B are independent random variables both sampled from normal distributions, were determined by calculating the probability distribution that $\rho(A, B)$ is a given nonzero value. For a given sample size (e.g., $N = 200$), MATHCAD was used to calculate the correlation coefficient for randomly drawn values of A and B (yielding, e.g., $\rho_{200}(A, B) = 0.074$). The calculation was repeated for 5000 trials, generating a sequence (e.g., 0.074, 0.053, 0.088, . . .) representing the various realized values of $\rho_{200}(A, B)$. These results then were sorted to provide a histogram of the number of times that a given value is found in the sequence, yielding a frequency curve that essentially is monotonically decreasing with increas-

ing values of ρ_{200}. The bounding values ρ_{200}^{-} and ρ_{200}^{+}, between which 95% of the realized outcomes of the calculation lie, then were noted.

This simulation was repeated for other values of N, and the smooth curve shown in Fig. 8 was generated. The abscissa represents the sample size (e.g., 216). The ordinate indicates the values $\{\rho_N^-, \rho_N^+\}$ for which, if $\rho_N^- < \rho_N < \rho_N^+$, one can say that the realized value is indistinguishable from zero (the idealized value for independent random variables) "with a confidence level of 0.95." For a sample size of $N = 216$ (i.e., the number of triskelion arms), these ρ_N^-, ρ_N^+ values are $\sim\pm0.13$, whereas if $N = 144$ (for tests involving the hub angles), the numbers are ±0.16.

A plot (also shown in Fig. 8) was obtained similarly for the tricorrelation coefficients given by Eq. C2. In this case, one finds that the 95% level of significance for a sample size of 72 triskelions ($N = 216$ arms) lies between -0.27 and 0.26; that is, if $|\rho_{s,72}(A)| \leq 0.27$, then the calculated tricorrelation coefficient is not significantly different from the value zero that would be obtained by sampling independently fluctuating random variables.

APPENDIX D

RIGIDITY ANALYSIS

$C(s)$ is related to a local shape function, $\theta(s)$, according to $C(s) = \partial\theta(s)/\partial s$. Let us now suppose that the shape function of an individual arm can be decomposed into a series of normal modes (Gittes et al., 1993; Käs et al., 1996)

$$\theta(s) = \sum_{n=0}^{\infty} \theta_n(s)$$

$$= (2L^{-1})^{1/2} \sum_{n=0}^{\infty} a_n \cos\left(\frac{n\pi s}{L}\right), \qquad \text{(D1)}$$

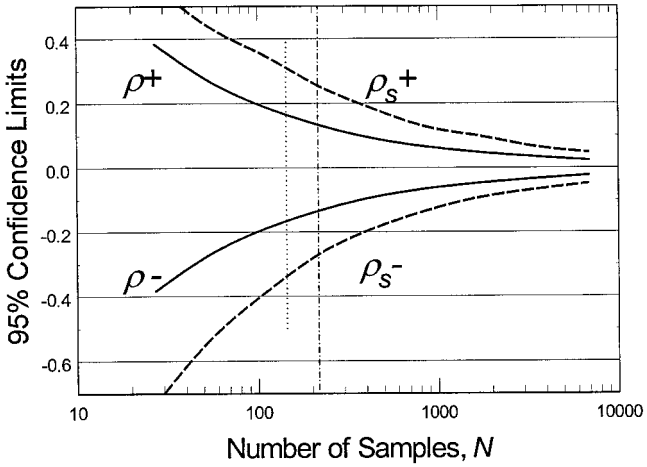

FIGURE 8 Values of $\rho_N^{\pm}(A, B)$ (*solid curves*) and $\rho_{s,N}^{\pm}(A1, A2, A3)$ (*dashed curves*). If $\rho_N^-(A, B) < \rho_N(A, B) < \rho_N^+(A, B)$ for a finite sample size N, one can presume, at a 95% confidence level, that the variables A and B are independent (see Eq. C1). Similarly (see Eq. C2), if $\rho_{s,N}^- < \rho_{s,N}(A1, A2, A3) < \rho_{s,N}^+$, where $A1$, $A2$, $A3$ are identical normal distributions, one can presume that $A1$, $A2$, $A3$ are independently fluctuating. Our triskelion sample set contains 216 arms and 144 independent hub angles (see vertical lines).

where L is the intrinsic length of an arm. Then, from Eq. 6, the variance in the amplitude of each mode, $\langle(a_n - a_n^0)^2\rangle$, is related to the flexural rigidity according to

$$\langle(a_n - a_n^0)^2\rangle = \frac{k_B T}{EI}\left(\frac{L}{n\pi}\right)^2, \qquad \text{(D2)}$$

so that, in principle, an analysis of the individual modes can give independent measures of EI. Equation D2 reflects the notion of equipartition of energy (Reif, 1965), which signifies that the energy associated with each mode excited by the thermal bath is equal to $\frac{1}{2}k_BT$.

To first order, the mode amplitudes and variances can be calculated from the triskelion images according to Eqs. A2–A4 as

$$a_n^{(i,j)} = \sum_{s=0}^{\mu(L)} \frac{(2\mu(L))^{1/2}}{50}\left[\alpha^{(i,j)}(s) \cdot \cos\frac{n\pi s}{\mu(L)}\right], \quad n = 1, 2, \ldots \qquad \text{(D3)}$$

and

$$\langle(a_n - a_n^0)^2\rangle = \frac{\sum_{i,j}^{N} (a_n^{(i,j)} - \mu(a_n^{(i,j)}))^2}{N - 1}, \qquad \text{(D4)}$$

where $N = 216$ is the total number of triskelion arms in our data set. In fact, though, our numerical data reduction is complicated by two factors: (1) an uncertainty in determining the node coordinates from the original electron micrographs (Kocsis et al., 1991) and (2) our spline-based fitting procedure (see Appendix A). The first progressively increases the amplitude variance for higher modes (Gittes, et al., 1993; Käs et al., 1996), whereas the second suppresses the absolute amplitude at higher mode numbers (especially those for $n \geq \frac{1}{2}n_m$, where n_m is the total number of spline nodes used to describe arm shape). Because our data analysis for arm shapes generally yields n_m values of 9 ± 1, these effects limit the useful normal modes to approximately the first 5. For the leading modes (i.e., small n), numerical modeling (data not shown) suggests that the combined effect of these two factors is to add an approximately constant background term to the $1/n^2$ behavior of Eq. D2, so we obtain the expression given in Eq. 7.

The authors thank Dr. E. Kocsis for providing the set of nodal coordinates of triskelions in electron micrographs and for explaining the procedures of image acquisition and digitization. We also thank Drs. J. Keen, K. Prasad, A. C. Steven, and B. L. Trus for helpful discussions.

REFERENCES

Anderson, R. G. W. 1998. The caveolae membrane system. *Annu. Rev. Biochem.* 67:199–225.

Brodsky, F. M. 1988. Living with clathrin: its role in intracellular membrane traffic. *Science.* 242:1396–1402.

Brodsky, F. M., B. L. Hill, S. L. Actin, L. Nathke, D. H. Wong, S. Ponnambalam, and P. Parham. 1991. Clathrin light chains: arrays of protein motifs that regulate coated-vesicle dynamics. *TIBS.* 16:208–213.

Crowther, R. A., and B. M. F. Pearse. 1981. Assembly and packing of clathrin into coats. *J. Cell. Biol.* 91:790–797.

Dell'Angelica, E. C., J. Klumperman, W. Stoorvogel, and J. S. Bonifacino. 1998. Association of the AP-3 adaptor complex with clathrin. *Science.* 280:431–434.

Elliott, A., G. Offer, and K. Burridge. 1976. Electron microscopy of myosin molecules from muscle and non-muscle sources. *Proc. R. Soc., Ser. B.* 193:43–53.

Elson, E. L. 1988. Cellular mechanics as an indicator of cytoskeletal structure and function. *Annu. Rev. Biophys. Biophys. Chem.* 17: 397–430.

Evans, E. 1983. Bending elastic modulus of red blood cell membrane derived from buckling instability in micropipet aspiration tests. *Biophys. J.* 43:27–30.

Frank, R. S. 1990. Time-dependent alterations in the deformability of human neutrophils in response to chemotactic activation. *Blood.* 76: 2606–2612.

Gittes, F., B. Mickey, J. Nettleton, and J. Howard. 1993. Flexural rigidity of microtubules and actin filaments measured from thermal fluctuations in shape. *J. Cell Biol.* 120:923–934.

Griffith, J., M. Bleyman, C. A. Rauch, P. A. Kitchin, and P. T. Englund. 1986. Visualization of bent helix in kinetoplast DNA by electron microscopy. *Cell.* 46:717–724.

Helfrich, W. 1973. Elastic properties of lipid bilayers: theory and possible experiments. *Z. Naturforsch.* 28c:693–703.

Heuser, J. E. 1989. Effects of cytoplasmic acidification on clathrin lattice morphology. *J. Cell. Biol.* 108:402–411.

Jin, A. J., and R. Nossal. 1993. Topological mechanisms involved in the formation of clathrin-coated vesicles. *Biophys. J.* 65:1523–1537.

Käs, J., H. Strey, J. X. Tang, D. Finger, R. Ezzell, E. Sackmann, and P. A. Janmey. 1996. F-actin, a model polymer for semiflexible chains in dilute, semidilute, and liquid crystalline solutions. *Biophys. J.* 70: 609–625.

Keen, J. 1990. Clathrin and associated assembly and disassembly proteins. *Annu. Rev. Biochem.* 59:415–438.

Keen, J. H., M. C. Willingham, and I. H. Pasten. 1979. Clathrin-coated vesicles: isolation, dissociation and factor-dependent reassociation of clathrin baskets. *Cell.* 16:303–312.

Kirchhausen, T., and S. C. Harrison. 1981. Protein organization in clathrin trimers. *Cell.* 23:755–761.

Kirchhausen, T., S. C. Harrison, and J. E. Heuser. 1986. Configuration of clathrin trimers: evidence from electron microscopy. *J. Ultrastruct. Res.* 94:199–208.

Kirchhausen, T., S. C. Harrison, E. Ping Chow, R. J. Mataliano, K. L. Ramachandran, J. Smart, and J. Brosius. 1987. Clathrin heavy chain: a molecular cloning and complete primary structure. *Proc. Natl. Acad. Sci. USA.* 84:8805–8809.

Kocsis, E., B. L. Trus, C. J. Steer, M. E. Bisher, and A. C. Steven. 1991. Image averaging of flexible fibrous macromolecules: the clathrin triskelion has an elastic proximal segment. *J. Struct. Biol.* 107:6–14.

Landau, L. D., and E. M. Lifshitz. 1959. Theory of Elasticity. Addison-Wesley, New York.

Lin, H. C., M. S. Moore, D. A. Sanan, and R. G. W. Anderson. 1991. Reconstitution of clathrin-coated pit budding from plasma membranes. *J. Cell. Biol.* 114:881–891.

Nossal, R. 1998. A thermodynamic model for clathrin basket assembly. *Biophys. J.* 74:95*a*(Abstr.).

Orlova, A., and E. H. Egelman. 1993. A conformational change in the actin subunit can change the flexibility of the actin filament. *J. Mol. Biol.* 232:334–341.

Oster, G. F., L. Y. Cheng, H.-P. H. Moore, and A. S. Perelson. 1989. Vesicle formation in the Golgi apparatus. *J. Theor. Biol.* 141:463–504.

Parton, R. G. 1996. Caveolae and caveolins. *Curr. Opin. Cell Biol.* 8:542–548.

Pastan, I., and M. C. Willingham, eds. 1985. Endocytosis. Plenum, New York.

Pearse, B. M. F., and M. S. Bretscher. 1981. Membrane recycling by coated vesicles. *Annu. Rev. Biochem.* 50:85–101.

Pearse, B. M. F., and R. A. Crowther. 1987. Structure and assembly of coated vesicles. *Annu. Rev. Biophys. Biophys. Chem.* 16:49–68.

Press, W. H., B. P. Flannery, S. A. Teukolsky, and V. T. Vetterling. 1988. Numerical Recipes. *In* C: The Art of Scientific Computing. Chap. 3. Cambridge University Press, New York.

Reif, F. 1965. Fundamentals of Statistical and Thermal Physics. McGraw-Hill, New York.

Rivetti, C. M. Guthold, and C. Bustamante. 1996. Scanning force microscopy of DNA deposited onto mica: equilibration versus kinetic trapping studied by statistical polymer chain analysis. *J. Mol. Biol.* 264:919–932.

Robinson, M. S. 1992. Adaptins. *Trends Cell Biol.* 2:293–297.

Robinson, M. S., C. Watts, and M. Zerial. 1996. Membrane dynamics in endocytosis. *Cell.* 84:13–21.

Sachs, L. 1978. Applied Statistics: A Handbook of Techniques. Springer-Verlag, New York.

Santini, F., M. S. Marks, and J. H. Keen. 1998. Endocytic clathrin-coated pit formation is independent of receptor internalization signal levels. *Mol. Biol. Cell.* 9:1177–1194.

Schekman, R., and L. Orci. 1996. Coat proteins and vesicle budding. *Science.* 271:1526–1533.

Schmid, S. L. 1993. Biochemical requirements for the formation of clathrin- and COP-coated transport vesicles. *Curr. Biol.* 5:621–627.

Schmid, S. L. 1997. Clathrin-coated vesicle formation and protein sorting: an integrated process. *Annu. Rev. Biochem.* 66:511–548.

Schmid, S. L., and E. Smythe. 1991. Stage-specific assays for coated pit formation and coated vesicle budding in vitro. *J. Cell. Biol.* 114: 869–880.

Seifert, U., and R. Lipowsky. 1995. Morphology of vesicles. *In* Structure and Dynamics of Membranes. R. Lipowski and A. Sackmann, editors. Chap. 8. Elsevier, Amsterdam.

Shotten, D. M., B. E. Burke, and D. Branton. 1979. The molecular structure of human erythrocyte spectrin. *J. Mol. Biol.* 131:303–329.

Smith, C. J., N. Grigorieff, and B. M. F. Pearse. 1998. Clathrin coats at 21 Å resolution: a cellular assembly designed to recycle multiple membrane receptors. *EMBO J.* 17:4943–4953.

Sweitzer, S. M., and J. E. Hinshaw. 1998. Dynamin undergoes a GTP-dependent conformational change causing vesiculation. *Cell.* 93: 1021–1029.

Takei, K., V. I. Slepnev, V. Haucke, and P. De Camilli. 1999. Functional partnership between amphiphysin and dynamin in clathrin-mediated endocytosis. *Nature Cell Biol.* 1:33–39.

Trus, B. L., and A. C. Steven. 1981. Digital image processing of electron micrographs—the PIC system. *Ultramicroscopy.* 6:383–386.

Ungewickell, E., and D. Branton. 1981. Assembly units of clathrin coats. *Nature (Lond.).* 289:420–422.

Vigers, G. P. A., R. A. Crowther, and B. M. F. Pearse. 1986. Location of the 100 kD-50 kD accessory proteins in clathrin coats. *EMBO J.* 5:2079–2085.

Woodward, M. P., and T. F. Roth. 1978. Coated vesicles: characterization, selective dissociation, and reassembly. *Proc. Natl. Acad. Sci. USA.* 75:4394–4398.

Ybe, J. A., F. M. Brodsky, K. Hofmann, K. Lin, S.-H. Liu, L. Chen, T. N. Earnest, R. J. Fletterick, and P. K. Hwang. 1999. Clathrin self-assembly is mediated by a tandemly repeated superhelix. *Nature (Lond.).* 339: 371–375.

Zaremba, S., and J. H. Keen. 1983. Assembly polypeptides from coated vesicles mediate reassembly of unique clathrin coats. *J. Cell Biol.* 97:1339–1347.

Zhelev, D. V., D. Needham, and R. M. Hochmuth. 1994. Role of the membrane cortex in neutrophil deformation in small pipettes. *Biophys. J.* 67:696–705.